Analysis of gamma rhythms in the rat hippocampus *in vitro* and *in vivo*

Roger D. Traub*†‡, Miles A. Whittington§, Simon B. Colling§, György Buzsáki‖ and John G. R. Jefferys§

*IBM Research Division, T. J. Watson Research Center, Yorktown Heights, NY 10598, USA, †Department of Neurology, Columbia University, New York, NY 10032, USA, §Department of Physiology and Biophysics, St Mary's Hospital Medical School, Imperial College, London W2 1PG, UK and ‖Centre for Molecular and Behavioral Neuroscience, Rutgers University, Newark, NJ 07102, USA

1. We have shown previously, with experimental and computer models, how a '40 Hz' (gamma) oscillation can arise in networks of hippocampal interneurones, involving mutual $GABA_A$-mediated synaptic inhibition and a source of tonic excitatory input. Here, we explore implications of this model for some hippocampal network phenomena in the rat *in vitro* and *in vivo*.

2. A model network was constructed of 1024 CA3 pyramidal cells and 256 interneurones. AMPA (α-amino-3-hydroxy-5-methyl-4-isoxazole propionic acid), NMDA (*N*-methyl-D-aspartate), $GABA_A$ and $GABA_B$ receptors were simulated on pyramidal cells and on interneurones.

3. In both model and experiment, the frequency of network oscillations, in the gamma range, depended upon three parameters: $GABA_A$ conductance and decay time constant in interneurone→interneurone connections, and the driving current to the interneurones.

4. The model of gamma rhythm predicts an average zero phase lag between firing of pyramidal cells and interneurones, as observed in the rat hippocampus *in vivo*. The model also reproduces a gamma rhythm whose frequency changes with time, at theta frequency (about 5 Hz). This occurs when there is 5 Hz modulation of a tonic signal to chandelier and basket cells.

5. Synchronized bursts can be produced in the model by several means, including partial blockade of $GABA_A$ receptors or of AMPA receptors on interneurones, or by augmenting AMPA-mediated EPSCs. In all of these cases, the burst can be followed by a 'tail' of transiently occurring gamma waves, a phenomenon observed in the hippocampus *in vivo* following sharp waves. This tail occurs in the model because of delayed excitation of the interneurones by the synchronized burst. A tail of gamma activity was found after synchronized epileptiform bursts both in the hippocampal slice (CA3 region) and *in vivo*.

6. Our data suggest that gamma-frequency EEG activity arises in the hippocampus when pools of interneurones receive a tonic or slowly varying excitation. The frequency of the oscillation depends upon the strength of this excitation and on the parameters regulating the inhibitory coupling between the interneurones. The interneurone network output is then imposed upon pyramidal neurones in the form of rhythmic synchronized IPSPs.

EEG rhythms at frequencies of 30–100 Hz are prominent in the hippocampus during the theta state (Soltesz & Deschênes, 1993; Bragin, Jandó, Nádasdy, Hetke, Wise & Buzsáki, 1995). Rhythms at similar frequencies occur in the neocortex, where they can be stimulus driven, and so are of possible significance for information processing (for review, see Gray, 1994).

It has been shown that gamma-frequency oscillations (used in this paper to mean frequencies at 20 Hz and above) can

‡To whom correspondence should be addressed at IBM.

be generated by networks of interneurones *in vitro* during blockade of ionotropic glutamate receptors, via mechanisms including tonic excitation of the interneurones, together with mutual $GABA_A$ receptor-mediated inhibition between the interneurones (Whittington, Traub & Jefferys, 1995*a*). Comparable network activity was observed in a model of mutually inhibitory neurones. An underlying mathematical idea, following Wang & Rinzel (1993), was that IPSPs can synchronize neuronal firing when the time course of synaptic inhibition is longer than the firing period exhibited by the synaptically uncoupled neurones. Certain CA1 stratum oriens and stratum pyramidale interneurones participate in *in vitro* gamma oscillations (Whittington *et al.* 1995*a*). Thus, for simulation purposes, we have assumed that basket and chandelier cells could be the generators of the gamma oscillation.

We suspect that *in vivo* gamma rhythms are generated within the hippocampus itself, as gamma frequency oscillations persist in the rat *in vivo* after subcortical denervation of the hippocampus, even when theta activity (4–12 Hz) is completely lost (Buzsáki, Gage, Czopf & Björklund, 1987). In addition, gamma activity in the CA3/CA1 regions also survives bilateral entorhinal cortex lesions (Bragin *et al.* 1995). The *in vivo* situation is complicated by the fact that theta- and gamma-frequency EEG rhythms co-exist in the hippocampus of the rat when awake or during ketamine–xylazine or urethane anaesthesia (Buzsáki, Leung & Vanderwolf, 1983; Soltesz & Deschênes, 1993; Bragin *et al.* 1995). Identified CA1 basket cells *in vivo* have been found to fire at gamma frequencies, in short bursts that are interrupted at theta frequencies (Ylinen, Soltész, Bragin, Penttonen, Sik & Buzsáki, 1995*b*). *In vitro* gamma oscillations are not, however, interrupted at theta frequency, suggesting that some input – to the interneuronal network generating gamma – is itself modulated at theta frequency.

These considerations motivated us to examine in more detail the parameters that control the frequency and patterning of an interneuronal network with mutual $GABA_A$ receptor-mediated inhibition. The results suggested that gamma oscillations might be elicited under certain conditions of synchronized pyramidal cell firing, and we present *in vitro* and *in vivo* data in support of this.

Some of these data have been presented in preliminary form (Whittington, Traub & Jefferys, 1995*b*; Traub, Jefferys, Whittington, Buzsáki, Pentonnen & Colling, 1995).

METHODS

Experimental methods *in vivo*

Recordings were made in male and female Sprague–Dawley rats, 300–450 g, using methods described in Ylinen *et al.* (1995*a*). Intracellular recordings were made in anaesthetized rats using 1·5 g kg^{-1} urethane. Entorhinal cortex lesions were made following the procedure described in Bragin *et al.* (1995). Briefly, the rats were anaesthetized with halothane (4% for induction, 1% for maintenance), and put into a stereotaxic apparatus. After the bone above the entorhinal cortex was removed and the dura incised, entorhinal tissue was removed by suction. The wound was filled with Gelfoam, the muscle flap re-attached and sutured, and the wound area treated with local antibiotics. Evoked responses to stimulation of the perforant path could be produced up to 14 days after bilateral removal of the entorhinal cortex, probably due to the slow degeneration of axons disconnected from their cell bodies.

Experimental methods *in vitro*

Transverse 400 μm-thick slices of dorsal hippocampus were prepared from brains removed from fourteen male Sprague–Dawley rats, 250–350 g, stunned and killed by cervical dislocation followed by decapitation. Slices were maintained in an interface recording chamber perfused with artificial cerebrospinal fluid (ACSF) containing (mM): NaCl, 135; $NaHCO_3$, 16; KCl, 3; $CaCl_2$, 2; NaH_2PO_4, 1·25; $MgCl_2$, 1; D-glucose, 10; equilibrated with 95% O_2–5% CO_2, pH 7·4 at 34 °C.

Gamma oscillations were evoked in slices in three ways. (1) Pressure ejection of 10 mM L-glutamate or 200 μM (1*S*,3*R*)-1-aminocyclopentane-1,3-dicarboxylic acid (ACPD), made up in the ACSF including any drugs that were also present (see below). Ejection was via glass micropipettes, 20–80 kΩ, onto the stratum pyramidale of area CA1 within 70 μm of the recorded cell. (2) Strong electrical stimulation, square wave, 50 μs duration, within 100 μm of the recorded cell, in the presence of 20 μM ACPD in the bathing solution. (3) Addition of 4-aminopyridine (4-AP, 70 μM) to generate synchronized burst discharges mimicking hippocampal sharp waves. For experiments using methods (1) and (2) above, $GABA_A$ receptor-mediated responses were isolated from other ionotropic responses by inclusion in the ACSF of the following: 6-cyano-7-nitroquinoxaline-2,3-dione (CNQX, 20 μM) or 6-nitro-7-sulphamoylbenzo[*f*]quinoxaline-2,3-dione (NBQX, 20 μM); D-2-amino-5-phosphonopentanoic acid (D-AP5, 100 μM) or 3-((*R*)-2-carboxypiperazin-4-yl)-propyl-1-phosphonic acid (CPP, 20 μM); 3-amino-2-(-4-chlorophenyl)-2-hydroxypropylsulphonic acid (2OH-saclofen, 0·2 mM). (In the absence of metabotropic glutamate receptor activation, CNQX and NBQX (both 20 μM) had slightly different effects on spontaneous IPSC frequency: 4–6 Hz for CNQX, about 2 Hz for NBQX. This effect is probably not significant for oscillations in the gamma frequency range.) For experiments using method (3) above, none of these drugs were added to the ACSF, but the ACSF was modified to promote bursting activity (Traub, Colling & Jefferys, 1995) (mM): NaCl, 124; $NaHCO_3$, 26; KCl, 5; $CaCl_2$, 2; $MgCl_2$, 1·6; NaH_2PO_4, 1·25; and D-glucose, 10.

Recordings were made of activity in both pyramidal cells and inhibitory interneurones located within stratum pyramidale, or in stratum oriens near to stratum pyramidale. Glass microelectrodes were filled with 2 M potassium methylsulphate, resistance 30–60 MΩ. Interneurones were identified physiologically by narrow action potentials (<3 ms at the base), lack of spike accommodation and by deep brief after-hyperpolarizations. For voltage clamp studies, electrodes also contained the lidocaine (lignocaine) derivative QX314, 50 mM. As QX314 took about 20 min to block action potentials, interneurones could still be identified physiologically when QX314 was in the electrode. Recordings were made in bridge mode or switched voltage clamp (Axoclamp 2B, 7–9 kHz, holding potential −40 mV) from forty-one pyramidal cells (31 from area CA3, 10 from area CA1) and eight inhibitory cells (all

CA1). Basic cell parameters were: input resistance 35–55 MΩ (CA1 and CA3 pyramidal cells) and 50–65 MΩ (interneurones, electrodes containing QX314); membrane potentials were −65 to −70 mV for pyramidal cells and −62 to −67 mV for interneurones (electrodes containing QX314).

Further pharmacological manipulations performed were bath application of: (1) bicuculline (0·5–5 μM) to reduce $GABA_A$ conductances (g_{GABA_A}); (2) thiopental (2–20 μM) to increase preferentially IPSC decay time constant (τ_{GABA_A}); (3) diazepam (50–500 nM) to increase preferentially IPSC size (Macdonald & Olsen, 1994; M. A. Whittington, unpublished data). In experiments using 4-AP, the partially specific metabotropic glutamate receptor antagonists L(+)-2-amino-3-phosphonopropionic acid (L-AP3, 0·2 mM), and (+)-α-methyl-4-carboxyphenylglycine ((+)-MCPG, 0·2 mM) were applied to the ACSF. All chemicals were obtained from Tocris Cookson, Bristol, UK.

Recordings were digitized and analysed using hardware and software from CED (Cambridge Electronic Design, Cambridge, UK). Principal oscillatory frequency was measured by performing autocorrelation analysis of trains of IPSCs and taking the reciprocal of the time to the first, largest peak of the autocorrelogram. IPSC decay constant was measured by fitting the decay phase of individual IPSCs within a train to a single-exponential function. $GABA_A$ conductance was estimated from the magnitude of the maximum evoked monosynaptic IPSC (not in a train) with a driving potential of 30 mV (holding potential of −40 mV). All data were analysed, where appropriate, using analysis of variance followed by Bonferroni's t test for multiple comparisons.

For analysis of gamma-frequency 'tails' following synchronized bursts induced by 4-AP, a waveform autocorrelation *vs.* time graph was constructed for each intracellular discharge, using a 500 ms bin width for the immediate post-burst after-hyperpolarization. Twenty to thirty events were analysed for each cell. The time to the first peak (if any) on the autocorrelation graph was measured and its reciprocal gave the frequency. The autocorrelation for some bursts had no peaks (i.e. no oscillation was present). For each cell, the number of bursts followed by an oscillation, divided by the total number of bursts analysed, was expressed as a percentage.

Simulation methods

Insufficient data are available to define a hippocampal network of truly realistic complexity. The computing resources do not exist to simulate a realistic network on a scale appropriate to the *in vivo* rat hippocampus. Compromises were necessary in both scale and complexity. We constructed a network of 1024 pyramidal cells and 256 inhibitory cells, which could be simulated on a parallel computer with sixteen nodes (processing units). There were fewer interneuronal subtypes in the model than actually exist (Gulyás, Miles, Hájos & Freund, 1993*a*; Buhl, Halasy & Somogyi, 1994), and the interconnection topology is undoubtedly oversimplified. The principles of the simulation are described in other papers: (1) most of the synaptic network simulation ideas are in Traub *et al.* (1995); (2) simulating a network of interneurones connected by gap junctions is described in Traub (1995); and (3) interneurones connected by $GABA_A$-ergic 'synapses' are described in Whittington, Traub & Jefferys (1995*a*). The following section describes what is specific to the present simulations.

Structure and intrinsic properties of individual neurones. Both model pyramidal cells and interneurones have branching dendrites, a soma and axon initial segment, and a short (4-compartment) stretch of axon. Model pyramidal neurones are intrinsically bursting cells, where bursts develop through interaction between predominantly perisomatic sodium conductance (g_{Na}) and predominantly dendritic high-threshold calcium conductance (g_{Ca}). Details are as in Traub, Jefferys, Miles, Whittington & Tóth (1994), with the exception that the after-hyperpolarization conductance ($g_{K_{AHP}}$) density has been decreased 25%. Model interneurones are, so far as intrinsic properties go, repetitively firing cells with little adaptation. We did not attempt to simulate the intrinsic oscillatory properties or burst properties recorded in some interneurones. Model interneurones have electrically excitable dendrites, in order to replicate the *in vitro* experimental observation that a single excitatory synapse, located in a dendrite, can evoke a short-latency action potential (Gulyás, Miles, Sik, Tóth, Tamamaki & Freund, 1993*b*; Sik, Tamamaki & Freund, 1993). As a consequence, the interneurone model predicts that under certain conditions action potentials may be initiated in dendrites, contrary to what appears to occur in pyramidal neurones (Traub *et al.* 1994; Spruston, Schiller, Stuart & Sakmann, 1995). Details of the interneurone model are given in Traub & Miles (1995).

Classification of model interneurones. As the model interneurones have identical intrinsic properties, they are classified according to their axonal distribution and postsynaptic actions. We consider that there are four types. (1) 'Chandelier cells' contact the initial segment of pyramidal cells, as well as the dendrites of interneurones (see below). The '$GABA_A$' postsynaptic conductance has a decay time constant, τ_{GABA_A}, of 10–13 ms. There are thirty-two chandelier cells. (2) 'Basket cells' contact, on pyramidal cells, the soma and those five dendritic compartments connected to the soma. They also contact interneurone dendrites. Default τ_{GABA_A} is 10 ms. There are sixty-four basket cells. (3) 'Dendritic' cells each contact four apical dendritic compartments in pyramidal cells, centred 180 μm from the soma, with τ_{GABA_A} 50 ms (Pearce, 1993; Traub *et al.* 1994). At this stage of the model, dendritic cells do not contact interneurones, owing to lack of data on this particular postsynaptic action. There are thirty dendritic cells. (4) '$GABA_B$' cells each contact the sixteen pyramidal apical dendritic compartments that are centred ⩾240 μm from the soma. They also contact interneurone dendrites. The time course of the unitary $GABA_B$ conductance was as described in Traub *et al.* 1994. There are 128 $GABA_B$ cells. Presynaptic $GABA_B$ receptors were not simulated.

Synaptic connectivity: dendritic location. Pyramidal→pyramidal synapses can occur either onto one of eight basilar dendritic compartments centered 35 μm from the soma, or onto one of twenty-four apical dendritic compartments centered 125–300 μm from the soma. Pyramidal→interneurone synapses can occur on short dendrites 75 μm or more from the soma, or on the longer dendrites 175 μm or more from the soma. Interneurone→interneurone connections are located on the most proximal dendritic compartments. As the electrotonic length of interneuronal dendrites is short (Thurbon, Field & Redman, 1994), the precise location of these synapses is unlikely to be critical.

Synaptic connectivity: number of release sites. For interneurone→pyramidal connections, the number of release sites depends on the type of the interneurone, as described above. For all other synaptic connections (that is, pyramidal→pyramidal, pyramidal→interneurone, and interneurone→interneurone), there is a single 'release site', in the sense that the connection is made to precisely one compartment of the postsynaptic neurone.

Synaptic connectivity: topology. Each pyramidal cell is contacted by thirty-two other randomly chosen pyramidal cells (connection probability = 32/1024 = 0·03125). Each interneurone is also contacted by thirty-two randomly chosen pyramidal cells, a low degree of connectivity (Miles, 1990). Each pyramidal cell is contacted by fifty interneurones, randomly chosen but subject to the constraint that there are ten presynaptic chandelier cells, twenty basket cells, ten dendritic cells and ten $GABA_B$ cells. Each interneurone is contacted by all ninety-six basket–chandelier cells (motivated by the estimate that a basket cell could contact as many as sixty other basket cells (Sik, Pentonnen, Ylinen & Buzsáki, 1995)), as well as ten randomly chosen $GABA_B$ cells. The simulations of the behaviour of the ninety-six interconnected basket–chandelier cells were repeated using a network of only sixteen interneurones with all–all connectivity; the results were qualitatively similar to those reported here.

Postsynaptic action. The time courses of inhibitory conductances are given above. Pyramidal→pyramidal connections engage both 'AMPA' and 'NMDA' conductances having the form of a conductance scaling constant × a function of time ($f(t)$) (and of $[Mg^{2+}]$ and membrane potential for the NMDA conductance). The pyramidal→pyramidal $f(t)$ for the AMPA conductance is $te^{-t/2}$ (t in milliseconds); for the NMDA conductance, $f(t)$ is $te^{-t/5}$ for the first 5 ms, followed by exponential decay with a time constant of 150 ms. The voltage and Mg^{2+} dependence of the NMDA conductance are as in previous publications (Traub, Whittington & Jefferys, 1994), using a default Mg^{2+} concentration of 2 mM.

Pyramidal→interneurone connections also engage AMPA and NMDA conductances, of faster time course than on pyramidal cells. The AMPA conductance is here proportional to te^{-t} and the NMDA conductance decays with a time constant of 60 ms (Perouansky & Yaari, 1993).

Conductance scaling constants. These parameters were often varied in different simulations, but we shall list the 'default' values. For AMPA conductances on pyramidal basilar dendrites, the value was 3 nS, and for apical dendrites 6 nS. Note that the standard conductance time course $f(t)$ has a maximum value of 0·736, so a unitary EPSC peaks at 2·21 or 4·42 nS; those are the dendritic conductances, which are higher than estimates from the soma during a voltage-clamp experiment. For NMDA conductances on pyramidal basilar dendrites, the scaling parameter was 1·0 nS, and on apical dendrites 8·0 nS. These pyramidal cell AMPA and NMDA conductances allow bursting to spread from neurone to neurone (Miles & Wong, 1987*a*), and allow after-discharges to occur during $GABA_A$ blockade (Traub, Miles & Jefferys, 1993). For AMPA conductances on interneurones, the scaling parameter was up to 8 nS, and for NMDA conductances 2 nS. The $GABA_A$ conductance on pyramidal cell initial segments was scaled by 1·5 or 2 nS; the basket cell-induced conductance was scaled by 3 or 4 nS (over all the postsynaptic compartments – i.e. the conductance was distributed over several compartments in proportion to their surface area); the dendritic $GABA_A$ conductance was scaled by 2·25 or 3 nS (over all the dendritic compartments). The pyramidal cell $GABA_B$ conductance was scaled by 0·5 nS over all the possible dendritic compartments. With the above inhibitory conductances, the network did not spontaneously generate epileptiform discharges. Interneurone→interneurone $GABA_A$ conductances were usually scaled by 0·5 nS. The interneurone→interneurone $GABA_B$ conductance scaling parameter could range from 0 to 3·0 nS.

Equilibrium potentials for synaptic conductances were as follows: 60 mV positive to rest for EPSPs; −15 mV relative to rest for IPSPs on pyramidal cells and $GABA_A$ IPSPs on interneurones; and −25 mV relative to rest for $GABA_B$ IPSPs on interneurones.

Postsynaptic conductances induced by trains of presynaptic action potentials. The general scheme is as described by Traub *et al.* (1995), except that here – for the sake of simplicity – interneurone-induced conductances do not facilitate or depress. Pyramidal cell-induced conductances first facilitate and then depress in a time-dependent way as outlined by Traub *et al.* (1995). The appropriately scaled and time-shifted unitary conductances are then added together to give the postsynaptic conductance. Finally, for certain conductances, a saturation rule is applied that maintains a maximum synaptic conductance for each compartment. Specifically, AMPA conductances per compartment cannot exceed 5 nS on pyramidal basilar dendrites or 15 nS on pyramidal apical dendrites; NMDA conductances per compartment on pyramidal basilar dendrites can not exceed 5 or 25 nS on apical dendrites; AMPA conductances per compartment on interneurones cannot exceed 8 nS or NMDA conductances 5 nS; $GABA_B$ conductances per compartment on pyramidal dendrites cannot exceed 0·15 nS. These parameters are somewhat arbitrary, but were chosen to be large enough to allow synchronized after-discharges to occur, and small enough to maintain numerical stability.

Synaptic noise was generated by ectopic axonal action potentials (Traub *et al.* 1995). Mean intervals between ectopic spikes in a given axon were 1 s for interneurones and 5 s for pyramidal cells.

Gap junctions occurred between dendrites of $GABA_B$ cells, with an average of two junctions per cell, and a junctional resistance of 150 MΩ. The gap junctions were non-rectifying and were permitted in six different compartments centred at 175 or 225 μm from the soma. At most, one gap junction could occur on a particular compartment of a particular cell. Inclusion of the gap junctions was motivated by the occurrence of large $GABA_B$-dependent potentials in media containing 4-AP together with blockers of AMPA, NMDA and $GABA_A$ receptors (Michelson & Wong, 1994; Traub, 1995).

Computing details. Programmes were written in FORTRAN augmented with parallel instructions and run on parallel computers: either IBM SP1s at the T. J. Watson Research Centre or an IBM SP2 at the Maui High Performance Computing Center. The parallel environment was euih and poe on the SP1, and poe alone on the SP2. The approach to simulating this type of network on a parallel computer is described elsewhere (Traub *et al.* 1995; Traub, 1995). The present network was partitioned among sixteen nodes as follows: sixty-four pyramidal cells per node and sixteen interneurones per node, with the $GABA_B$ cells on the 'high' nodes. Each node contains an identical copy of the synaptic and gap junctional 'wiring diagram'. In this way, simulations of interneuronal network activity with $GABA_B$ receptors blocked could be run on only the 'lower' eight nodes. In addition, only five pyramidal cells per node were used in the simulations when synaptic excitation was blocked, such pyramidal cells serving to register the output of the interneurone networks rather than to generate output themselves. Simulations on eight nodes, with five pyramidal cells per node, took about 5 h of elapsed time per second of neuronal time. Simulations of the full network on sixteen nodes took about 21 h of elapsed time per second of neuronal time.

RESULTS

Parameters controlling the gamma rhythm

The three parameters examined were: (a) in simulations, the mean *driving current* to interneuronal somata (using a uniform distribution across the ninety-six-member basket–chandelier population, and a range of 0·01 nA); while in experiments, the *glutamate dose* was titrated; (b) τ_{GABA_A} (the time constant of $GABA_A$ IPSC decay at interneurone→interneurone connections); and (c) the conductance of the unitary $GABA_A$ IPSC at interneurone→interneurone connections. Each of these three parameters was investigated experimentally using pressure ejection of glutamate (see Methods).

Dependence of network frequency on driving current

In the model, network frequency depends linearly on the driving current (Fig. 1). In the hippocampal slice, in the absence of ionotropic glutamate and $GABA_B$ receptor-mediated events, network frequency (measured in pyramidal cells) depends upon the duration of glutamate application, presumably determining the degree of activation of metabotropic glutamate receptors (Fig. 1, inset). Interestingly, in the experiment, network frequency first increases with glutamate pulse duration, then declines. The simplest explanation for this is that longer applications of glutamate activate increasing numbers of interneurones (hence increasing inhibition between the interneurones), as well as providing greater stimulation to a subset of interneurones. Such a spatial non-uniformity of drug action is not simulated in the model. The frequency decline might also reflect heterogeneity in metabotropic receptor types and/or actions (see Discussion).

Dependence of network frequency on τ_{GABA_A}

In Fig. 2, we replicate an earlier result (Whittington *et al.* 1995*a*) that interneurone network frequency declines with increasing τ_{GABA_A}. In the experiment, thiopental was used to prolong τ_{GABA_A} as measured in stratum pyramidale–

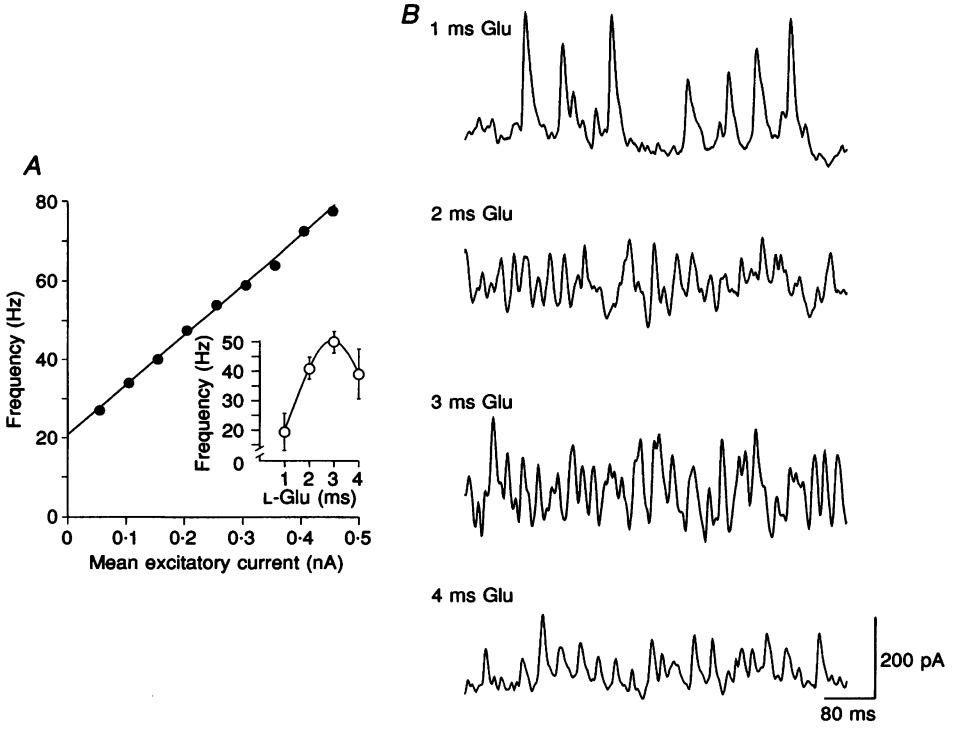

Figure 1. Dependence of interneuronal gamma oscillation on driving current

A, we simulated the subnetwork of 96 basket–chandelier interneurones, with all–all synaptic ($GABA_A$-mediated) connectivity. The range of driving currents across the population was 0·01 nA for each simulation. With τ_{GABA_A} fixed at 10 ms, network frequency increased from about 25 to over 70 Hz as the driving current was increased. Inset demonstrates the effect of increasing amounts of glutamate applied to the stratum pyramidale of the hippocampal CA1 region *in vitro*. Glutamate was applied by pressure ejection of 10 mM L-glutamate in ACSF containing drugs to block ionotropic glutamatergic transmission and $GABA_B$ receptor-mediated transmission (see Methods). Oscillation frequency was measured in CA1 pyramidal cells voltage clamped at −40 mV, using autocorrelation as described in Methods. Data are expressed as means ± S.E.M. ($n = 6$). Maximum evoked frequency was 49 ± 3 Hz. *B*, example current oscillations for the inset in *A*. In this and the next 3 figures, experimental data were low-pass filtered at 1 kHz and digitized at 2 kHz.

oriens interneurones. The model network is able to oscillate at lower frequencies than in the previous study, possibly a consequence of the higher network connectivity now used. The fit of the model to experiment is good, although increasing τ_{GABA_A} still does not cause the model to generate stable oscillations at frequencies as low as can be obtained experimentally. At higher doses, however, an appreciable effect of thiopental on IPSC conductance is seen, as well as an effect on τ_{GABA_A}, causing a further decrease in oscillation frequency for a given τ_{GABA_A}. The example traces demonstrate the type of IPSC train seen in control conditions (*a*) and in the presence of thiopental (*b*), the corresponding frequencies being 38 and 17 Hz.

Dependence of network frequency on $GABA_A$ conductance

This parameter was measured in stratum pyramidale interneurones and was manipulated experimentally by: (a) using increasing concentrations of bicuculline to decrease the parameter; and (b) increasing concentrations of diazepam to increase the parameter. Again, the fit of model to experiment is good (Fig. 3), with only a few experimental data points lying below the best-fit line in the presence of diazepam. These points probably reflect the ability of diazepam to increase τ_{GABA_A} as well as increasing conductance (about 14% increase in τ_{GABA_A} at 20 Hz population frequency).

Minimum network frequency

When τ_{GABA_A} is fixed in the 9–13 ms range, the network (simulated and experimental) does not oscillate at frequencies much below about 20 Hz, even as driving current or $GABA_A$ conductance are manipulated (Figs 1, 3 and 4). The reason can be understood as follows. Suppose $\tau_{GABA_A} = 10$ ms. With a network frequency of 20 Hz (period, 50 ms $= 5 \times \tau_{GABA_A}$), at the end of a period the compound IPSC will be reduced by a factor of e^5, or 148-fold. Such a small residual IPSC will not be able to entrain the population, and the network oscillation will not be stable. This argument, however, is not sufficient to predict

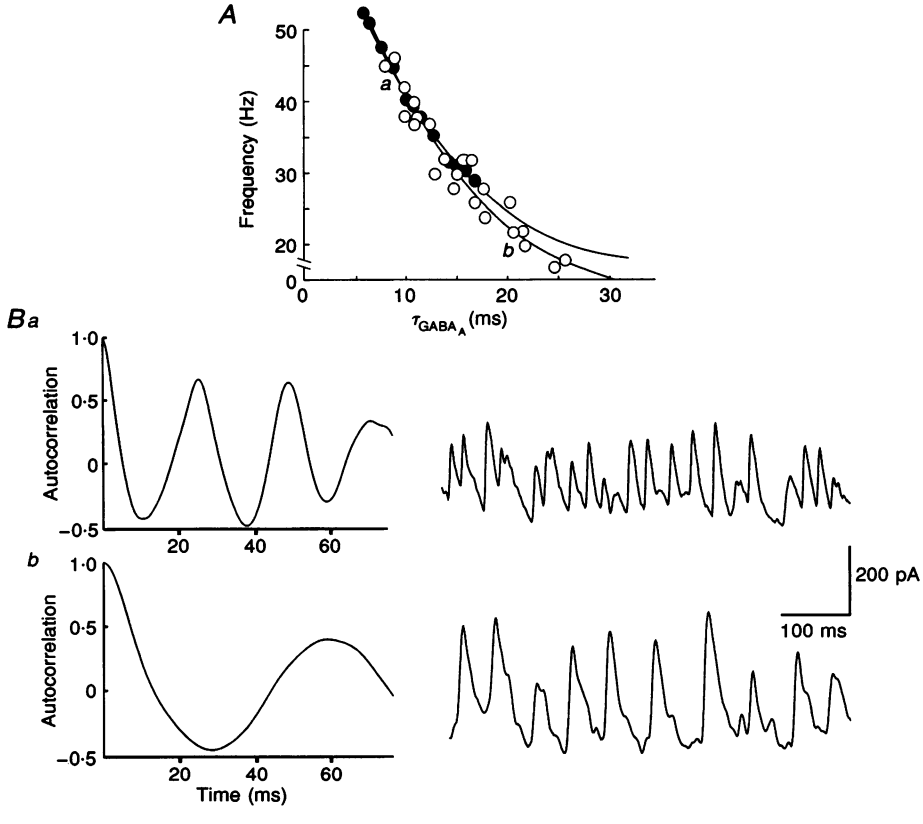

Figure 2. Dependence of interneuronal gamma oscillation on $GABA_A$ time constant

A, simulations (●) as in Fig. 1, but with driving currents fixed and τ_{GABA_A} varied. Experimental data (○) were obtained from 2 stratum pyramidale interneurones, recording in voltage clamp (holding potential, −40 mV), using pressure ejection of L-glutamate as in Fig. 1. Paired measurements of IPSC train frequency and τ_{GABA_A} within each train were made during the wash-in of 2–20 μM thiopental. (Recordings taken in ACSF with drugs to block ionotropic glutamate and $GABA_B$ receptor transmission, see Methods.) Network frequency decreased as τ_{GABA_A} increased, as shown before (Whittington *et al.* 1995*a*). *B*, example IPSC trains with autocorrelation analyses in the absence of thiopental (*a*) and during wash-in (*b*).

quantitatively what the minimum frequency will be in a particular case: the speed with which entrainment is lost will also depend on the dispersion of driving currents, and on the amount of noise.

Phasic input to the interneurone network

A prediction of Fig. 1 is that if the driving currents to an interneuronal network vary slowly enough, and if the currents stay above a threshold value, then the network should produce an output whose frequency is time dependent. Figure 4 illustrates an example of this. The simulation was performed with recurrent excitation and $GABA_B$ receptors blocked, and without drive to the dendritic $GABA_A$ cells. In the simulation (Fig. 4*A*), the driving current to each basket–chandelier cell began in the range 0·34–0·40 nA, decaying exponentially (time constant 350–375 ms) to final values of −0·06 to 0·0 nA. The initial network frequency is about 75 Hz, and the last interval where there is detectable synchrony has a frequency of 22 Hz, consistent with the data above. In the experiment (Fig. 4*B* and *C*), oscillations were induced in a hippocampal slice (bathed in NBQX, 20 μM; CPP, 20 μM; 2OH-saclofen, 0·2 mM; and ACPD, 20 μM), by electrical stimulation using a nearby stimulating electrode. Synaptic ($GABA_A$-induced) currents were recorded, in single-electrode voltage clamp, from a CA1 stratum pyramidale interneurone. The interneurone was physiologically identified (see Methods). The stimulus generates a monosynaptic IPSC followed by a train of smaller IPSCs. Again, the frequency declines with time, with the last well-defined frequencies lying between 17 and 20 Hz. The decline in power with time (Fig. 4*C*) is not surprising because, as the interneurones slow their firing rates, they are expected to fire out of phase with one another (see argument above).

The simulation of Fig. 4*A* predicts that a pyramidal cell – tonically excited – fires on the depolarizing peaks of the synaptically induced waves, as expected. Thus, the phase lag between pyramidal cell firing and interneurone firing is, on average, *zero* – a consequence of the fact that pyramidal cells and interneurones are 'clocked' by the same network IPSCs. This result is consistent with *in vivo* observations (Fig. 10 of Bragin *et al.* 1995).

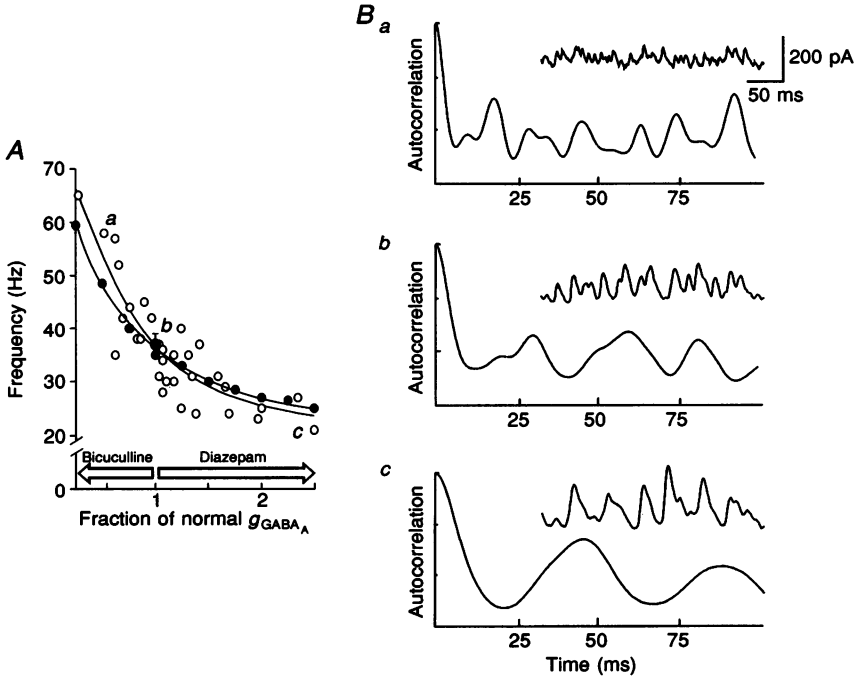

Figure 3. Dependence of interneuronal gamma oscillation on $GABA_A$ conductance (g_{GABA_A})
A, we simulated (●) the subnetwork of 96 chandelier–basket cells, with all–all synaptic ($GABA_A$-mediated) connectivity, as in Fig. 1. The range of driving currents was 0·15 to 0·16 nA for each simulation, and τ_{GABA_A} was 13 ms. Experimental points (○) are the principal frequency of oscillation in trains of IPSCs in stratum pyramidale interneurones after pressure ejection of L-glutamate (10 mM), plotted against GABA conductance estimated from the size of monosynaptic IPSCs evoked while the cell was held at −40 mV (recordings taken in ACSF with drugs to block ionotropic glutamate and $GABA_B$ receptor transmission, see Methods). $GABA_A$ conductance was increased by bath application of diazepam 0·05–0·5 μM, and decreased by bath application of bicuculline 0·5–5·0 μM. The large filled circle with error bars represents mean ± S.E.M. of oscillation frequency in control conditions ($n = 6$ observations). *B*, example recordings and autocorrelation analyses in the presence of 3 μM bicuculline (*a*), in controls (*b*), and in the presence of 0·5 μM diazepam (*c*).

Figure 5 illustrates a simulation in which the driving current to the basket–chandelier cells is sinusoidally modulated (period 200 ms), with a spread of 10% across the population in peak driving current amplitudes. The somatic potentials of eight basket cells are shown superimposed. The model can thus account for synchronized gamma-frequency oscillations that occur in short runs, in a pattern similar to that observed experimentally (Ylinen *et al.* 1995*b*). Note that action potential synchrony is diminished at the end of some of the runs (2nd and 3rd in Fig. 5).

Gamma oscillations following synchronized pyramidal cell bursts *in vitro*

Up to this point, we have simulated gamma oscillations by applying tonic, or slowly varying, depolarizing currents to basket–chandelier interneurones; the oscillation then emerges by virtue of the mutual $GABA_A$ synaptic interactions in the interneuronal pool (Whittington *et al.* 1995*a*). It seems possible that a transient gamma oscillation might emerge from: (a) an NMDA receptor-mediated excitation of the interneurone pool, given that NMDA receptors exist on interneurones (Sah *et al.* 1990; Traub *et al.* 1994) and gate currents with relatively slow time course (τ about 60 ms – Perouansky & Yaari, 1993); or (b) a metabotropic glutamate receptor-mediated excitation of the interneurones (Miles & Poncer, 1993; McBain, DiChiara & Kauer, 1994; Poncer, Shinozaki & Miles, 1995), a type of synaptic action not explicitly included in our network model.

In order to address this question, we simulated burst synchronization induced in three different ways: (a) partial blockade of $GABA_A$ receptors (Miles & Wong, 1987*a*); (b) an increase in the amplitude and duration of pyramidal cell EPSCs, along with ectopic axonal action potentials, in an attempt to replicate some of the actions of 4-AP (Traub *et al.* 1995); (c) partial blockade of AMPA receptors on

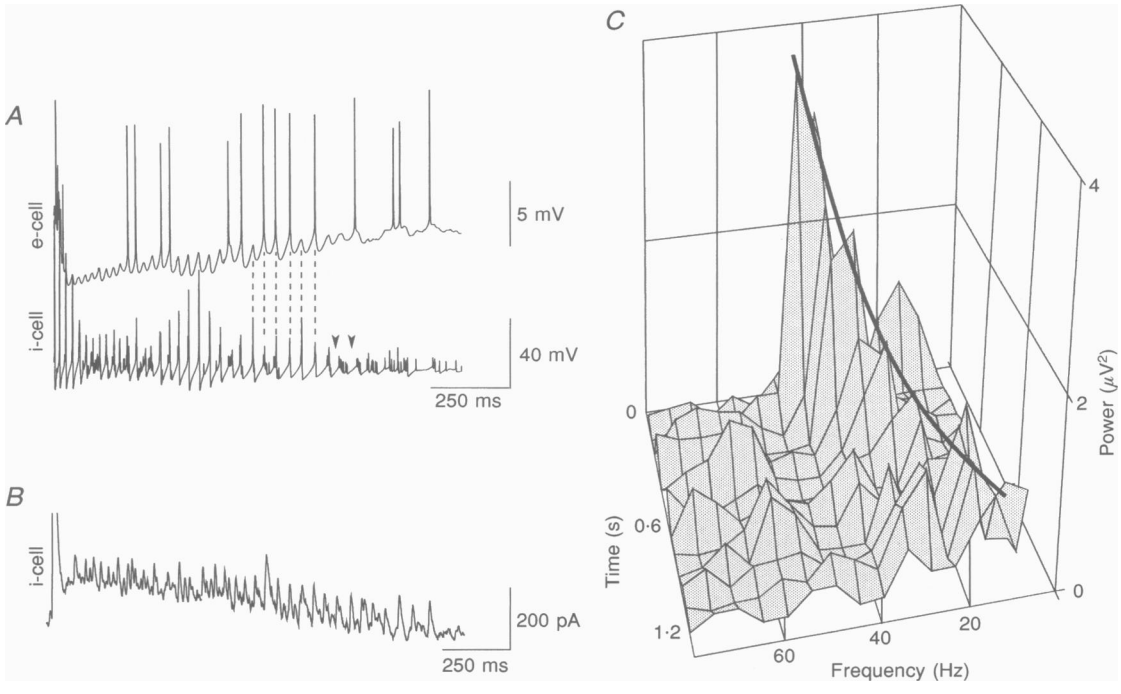

Figure 4. Response of the network when interneurones receive a transient stimulus

A, simulation. An exponentially decaying current was injected into the basket–chandelier interneurones, stimulus parameters as in the text. Recurrent excitation and $GABA_B$ were blocked. The basket–chandelier cell network generates an oscillation of gradually decreasing frequency until synchrony is lost; the last 2 intervals where there is synchrony (arrowheads) correspond to 38·5 and 22 Hz. We plot an average somatic voltage of 8 pyramidal cells ('e-cells') and 16 basket cells ('i-cells'). One of the pyramidal cells receives a constant 'afferent' input (18 nS into proximal apical dendrites) that causes it to fire. Note that pyramidal cell action potentials and interneuronal action potentials are tightly phase locked with zero phase difference, a result of the fact that both neuronal populations are 'clocked' by the same IPSPs. *B*, experimental oscillations measured in an interneurone following electrical stimulation in the presence of 20 μM ACPD (together with drugs to block ionotropic glutamate and $GABA_B$ receptor transmission, see Methods). Monosynaptic, maximal IPSC is truncated for clarity of the IPSC train (note different time scale from simulation in *A*). Maximum frequency was 46 Hz, minimum frequency terminating the IPSC train was 17 Hz. *C*, power spectrum analysis of trace in *B* (400 ms window) taken every 100 ms along the trace, to demonstrate both the decrease in power of the oscillation and the slowing of frequency.

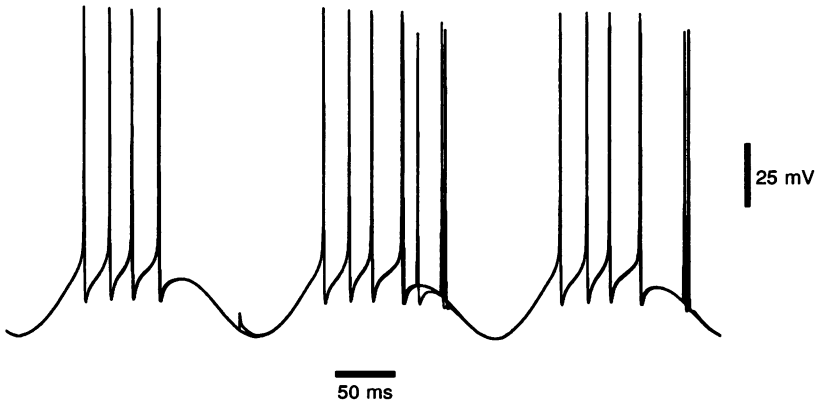

Figure 5. Simulated network response of basket–chandelier cells to a driving current sinusoidally modulated at theta frequency (5 Hz)

Superimposed somatic potentials of 8 basket cells are plotted, demonstrating synchrony of gamma-frequency firing in bursts, alternating with intervals of hyperpolarization (compare Ylinen *et al.* 1995*b*). Driving currents to the neurones were, in nA, $I \times \sin((2\pi t)/200)$, where I varied from 0·30 to 0·33 for different cells, and t is in ms. τ_{GABA_A} was 13 ms.

interneurones ('interneurone disconnection': Sloviter, 1991; Whittington & Jefferys, 1995). In all three cases, it was possible to obtain a transient gamma oscillation following the synchronized burst, but with partial $GABA_A$ blockade, the gamma activity was sensitive to parameter choice. The reason is that, for the gamma activity to occur, the interneurones must be driven by the synchronized firing of a sufficient number of pyramidal neurones. This requires, in turn, sufficient reduction of $GABA_A$ conductances. On the other hand, excessive reduction of $GABA_A$ conductances prevents the interneurones from synchronizing with each other (in the gamma frequency range), and also prevents observation of the oscillation in pyramidal cells. Partial blockade of pyramidal cell→interneurone synapses (without also blocking pyramidal→pyramidal synapses) is difficult to obtain in the acute *in vitro* slice, although tetanic stimulation may achieve this effect transiently (Miles & Wong, 1987*b*). We shall therefore concentrate on the 4-AP experimental model.

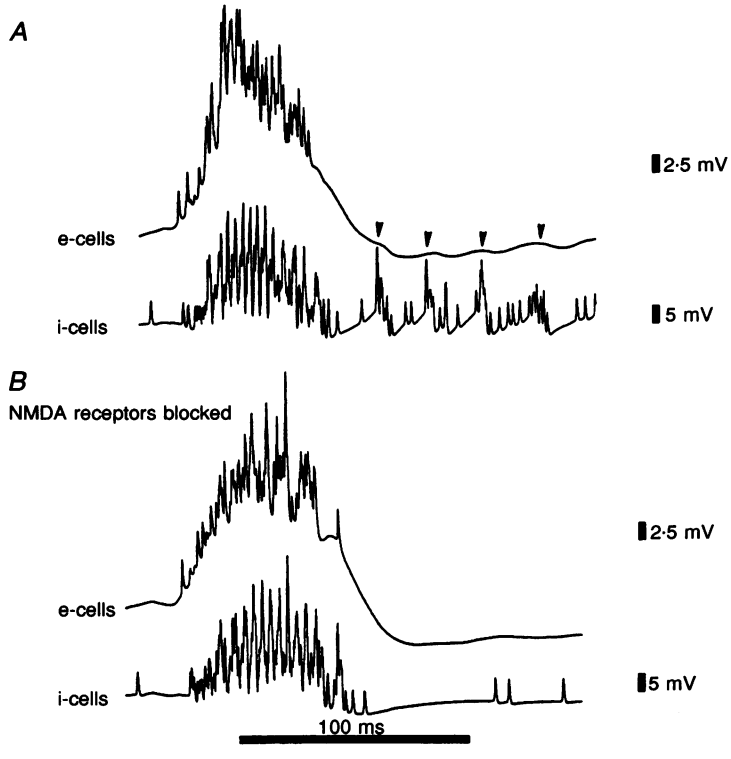

Figure 6. A gamma-frequency tail, dependent on NMDA receptor activation of interneurones, follows simulated 4-AP-induced synchronized bursts

The actions of 4-AP were simulated by increasing τ_{AMPA} at e→e (pyramidal cell→pyramidal cell) connections from 2 to 4 ms; see also text. The gamma tail appears as partially synchronized action potentials in the i-cell (interneurone) population following the burst, at frequencies 40–46 Hz, and as an undulating ripple in the pyramidal cell voltage (arrowheads in *A*, absent in *B*). Parameters in *B* identical to *A* except for blockade of NMDA receptors. Note the prominent high-frequency rippling in the i-cell signal during the synchronized burst. Average somatic potentials of 16 pyramidal cells ('e-cells') and 16 interneurones ('i-cells') plotted. Ectopic axonal spikes occur, on average, one every 5 s per pyramidal cell axon.

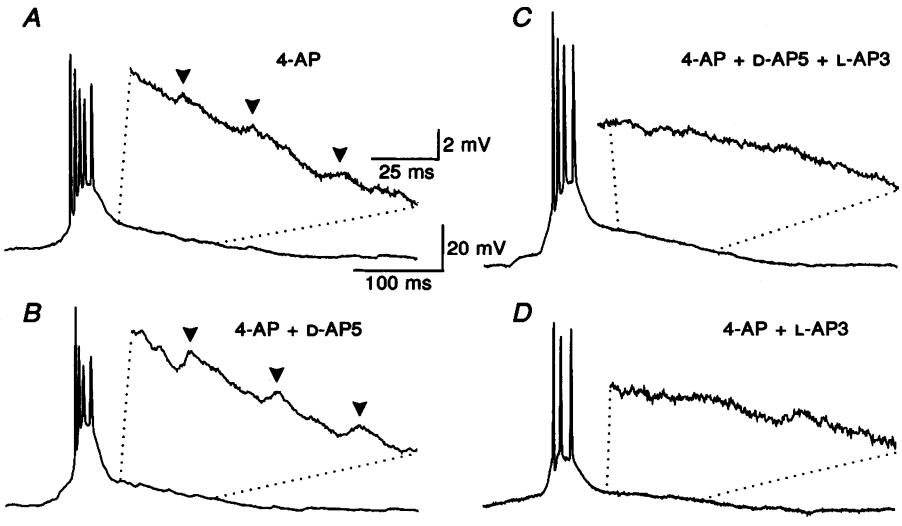

Figure 7. Gamma-frequency tails following 4-AP-induced synchronized bursts in CA3 region *in vitro*

Example traces recorded from the CA3b/c pyramidal cell region. Cells were maintained at the resting membrane potentials (see Methods). *A*, tail of gamma activity following a synchronized burst induced by 4-AP (70 μM). *B*, gamma activity remains under NMDA receptor blockade by D-AP5 (50 μM). Incidence of these gamma tails was slightly reduced (Fig. 8). *C* and *D*, blockade of metabotropic glutamate receptors by L-AP3 (0·2 mM) suppresses the gamma activity, both in the presence and absence of NMDA receptor blockade. Signals were low-pass filtered at 2 kHz and digitized at 5 kHz.

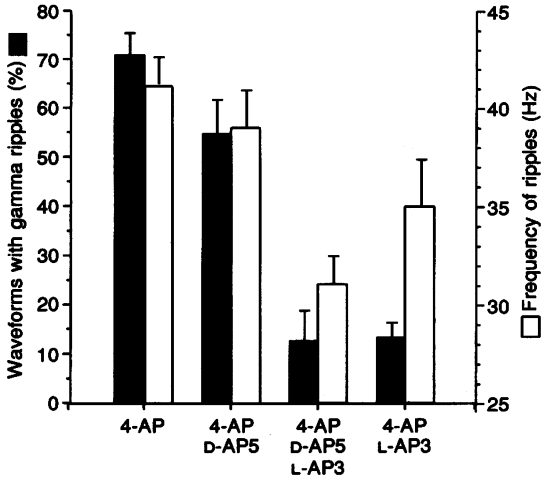

Figure 8. Incidence (■) and frequency (□) of gamma tails following 4-AP-induced synchronized bursts: metabotropic glutamate receptor blockade, but not NMDA receptor blockade, suppresses the tail

Gamma-frequency tails followed the 4-AP-induced synchronized bursts in 71 ± 5% of examples. The mean frequency of these rhythms was 41 ± 2 Hz. Gamma-frequency tails were still present following blockade of NMDA receptors by 50 μM D-AP5, although there was a slight decrease in their incidence to 55 ± 7% ($P > 0{\cdot}05$). The gamma-frequency tails were almost entirely abolished by blockade of metabotropic glutamate receptors by L-AP3 (0·2 mM; $P < 0{\cdot}02$). Under these conditions, only 13 ± 6% of bursts were followed by gamma-frequency tails, the mean frequency of the rhythms being reduced to 31 ± 1 Hz ($P < 0{\cdot}05$). This suppression of the gamma-frequency tails also occurred in the absence of NMDA receptor blockade, shown by the addition of L-AP3 alone ($P < 0{\cdot}0001$).

Figure 6*A* illustrates a simulation of a 4-AP-induced synchronized burst (see also Traub *et al.* 1995). During the synchronized burst itself, interneurones exhibit a large underlying synaptic depolarization and fire at high frequencies. Immediately *after* the synchronized burst, however, interneurones generate a partially synchronized network oscillation at 40–46 Hz, a result of the delayed excitation produced by pyramidal cell firing. This network oscillation is a result, in the model, of NMDA receptor-mediated excitation of the interneurones (Fig. 6*B*), and the interneurone network oscillation induces rhythmic membrane fluctuations in the pyramidal cells (arrowheads in Fig. 6*A*).

Such a membrane oscillation at gamma frequency was also observed experimentally in the pyramidal cell after-potentials following 4-AP-induced synchronized bursts (4-AP 70 μM), with mean frequency 41 $\pm$ 2 Hz ($n = 7$; Figs 7*A* and 8). Unlike the model, the experimental oscillations were not blocked by NMDA receptor blockade (D-AP5, 50 μM, Figs 7*B* and 8). There was a decrease in the mean incidence of oscillation following D-AP5 application, but this was not significant ($P > 0{\cdot}05$, $n = 6$). On the other hand, the non-specific metabotropic glutamate receptor blocker L-AP3 (0·2 mM), in combination with D-AP5 (50 μM), significantly reduced the incidence of the gamma ripples (Figs 7*C* and *D* and 8; $P < 0{\cdot}01$, comparison between oscillation seen in the presence of 4-AP and D-AP5 with ($n = 5$) or without L-AP3 ($n = 6$)). L-AP3 alone significantly decreased the percentage incidence of oscillations from 71 $\pm$ 5% (4-AP alone, $n = 7$) to 14 $\pm$ 3% (4-AP + L-AP3, $n = 7$, $P < 0{\cdot}0001$). The competitive metabotropic glutamate antagonist MCPG also significantly decreased the incidence of oscillations to 25 $\pm$ 5% ($n = 6$, $P < 0{\cdot}0001$). These data suggest that synchronized pyramidal cell bursts may be followed by a transient interneurone network oscillation, at gamma frequencies, and triggered in part by metabotropic glutamate receptor activation (as in *in vitro* experiments with ionotropic glutamate receptor blockade, Whittington *et al.* 1995*a*).

Gamma oscillation following synchronized pyramidal cell firing *in vivo*

Figure 9 illustrates, in recordings taken from the hippocampus of awake behaving rats, two examples of gamma oscillations following synchronized pyramidal cell firing. The first example (Fig. 9*A*) is a recording from a rat 4 days following a bilateral entorhinal cortex lesion, a lesion leading to frequent sharp waves that often – as in this example – occur in doublets. Single, but especially double, sharp wave bursts could be followed by a gamma 'tail' (Fig. 9*A*). Gamma 'tails' are also sometimes observed following sharp waves in normal awake behaving rats (G. Buzsáki, unpublished data).

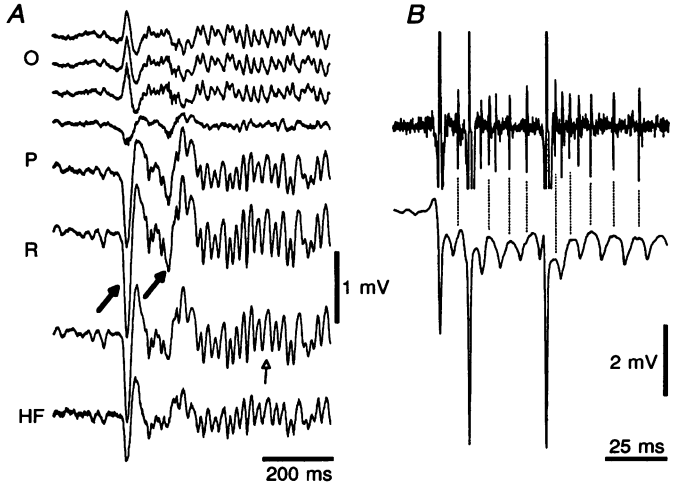

Figure 9. *In vivo* recordings: gamma activity following sharp waves and during a paroxysmal event

A, sharp wave (SPW, filled arrows) induced gamma oscillation in the CA1-dentate gyrus axis recorded 4 days after bilateral entorhinal cortex lesion. Note the high frequency (30–60 Hz) oscillatory tail (open arrow) triggered by the SPWs. *B*, population spike-associated gamma oscillation and interneuronal activity during paroxysmal event, induced by tetanic stimulation of the perforant path in an unlesioned rat. Upper trace: filtered derivative (0·5–10 kHz) of wide band; bottom trace: 1 Hz–10 kHz extracellular recording from the CA3c region of the hippocampus. The interneurone was physiologically defined as a fast firing (>10 Hz) cell which followed tetanic (200 Hz) stimulation of the perforant path. Note that the interneurone fired mostly on the positive part of the gamma oscillation (dashed lines). Recordings were taken from awake, freely moving rats. Abbreviations: O, s. oriens; P, s. pyramidale; R, s. radiatum; HF, hippocampal fissure.

The second example (Fig. 9*B*) was recorded from the CA3 region of an unlesioned rat, following a 1 s 200 Hz train to the contralateral fimbria-fornix, thereby inducing paroxysmal events with large (up to 25 mV) population spikes. An interneurone unit (the smaller unit in the upper trace, which was filtered at 0·5–10 kHz) was physiologically identified by its: (1) fast discharges (> 10 Hz) during theta activity prior to the paroxysmal event, (2) ability to follow 200 Hz stimulating trains; and (3) ability to respond repetitively to single-pulse commissural stimulation. During the paroxysmal event, pyramidal cells fired exclusively in association with the population spikes (not shown). Interneurones, on the other hand, fired both before and after the population spikes. As shown in Fig. 9*B*, the action potentials of the illustrated interneurone were tightly phase locked to extracellular gamma activity.

DISCUSSION

We have previously described a synchronized inhibitory neuronal oscillation, arising through mutual $GABA_A$ receptor-mediated inhibition in networks of commonly excited interneurones (Whittington *et al.* 1995*a*). Let us call this oscillation 'interneuronal network gamma', even though the frequencies involved extend into the 'beta' range (around 20 Hz). We showed, in the CA1 region of rat hippocampal slices, that interneurone network gamma did not require phasic synaptic input from pyramidal neurones, that interneurone network gamma could be evoked by metabotropic glutamate receptor activation, and that interneurone network gamma was suppressed by $GABA_B$ receptor activation. A primary purpose of the present study was to further define the mechanisms involved in interneurone network gamma, particularly those regulating its frequency, and to study when interneurone network gamma can occur in larger networks containing pyramidal cells as well as interneurones. Our data suggest the following properties of interneurone network gamma.

(1) The frequency of gamma oscillations can be regulated by a number of factors (Figs 1–3), including: (a) the time constant of $GABA_A$ IPSCs on interneurones (as previously shown, Whittington *et al.* 1995*a*); (b) the amplitude of IPSCs on interneurones; and (c) the driving currents to interneurones. The latter factor is not straightforward to analyse experimentally, possibly because of competing effects of different metabotropic glutamate receptor subtypes (Poncer *et al.* 1995), or of multiple 'downstream' effects produced by activation of a single receptor subtype. Spatial inhomogeneities of glutamate action on the interneurone population must also be considered.

(2) When τ_{GABA_A} is held constant, there is a minimum stable interneurone network gamma frequency. When τ_{GABA_A} is 10 ms, this minimum frequency is about 20 Hz with the other parameters we used (Fig. 4).

(3) Interneurone network gamma frequency can be 'tuned' when driving currents vary slowly enough (Figs 4 and 5). This property allows hippocampal interneurones to express gamma and theta rhythms at the same time, with gamma-generating cells firing in bursts (as occurs experimentally: Buzsáki *et al.* 1983; Bragin *et al.* 1995; Ylinen *et al.* 1995*b*).

(4) During interneurone network gamma, the firing of pyramidal neurones and interneurones should occur with zero (or small) phase-lag (Fig. 4). There is direct experimental confirmation of this prediction (Fig. 10 of Bragin *et al.* 1995).

(5) Interneurone network gamma can be evoked following a synchronized pyramidal cell burst – provided that $GABA_A$ receptors are not excessively blocked. This model prediction is supported by *in vitro* data using 4-AP as an epileptogenic agent (Figs 7 and 8), and by *in vivo* data after sharp waves and during paroxysmal events (Fig. 9). Following a 4-AP-induced burst or following a physiological sharp wave, the gamma activity is transient; this is unlike the sustained 'fast' activity following hippocampal seizures *in vivo* (Leung, 1987). While the model generates a gamma tail via NMDA receptor-mediated excitation of the interneurone pool (Fig. 6), experiments suggest that metabotropic glutamate receptor activation contributes, and that NMDA receptor-mediated excitation might not be critical for this phenomenon (Fig. 7). What is important in the model is not the receptor type; rather, it is the amplitude and slow time course of the putative slow EPSP produced in interneurones by the synchronized firing of pyramidal cells. It is interesting that L-AP3 reduced the gamma tail following a 4-AP-induced burst, whereas McBain *et al.* (1994) and Poncer *et al.* (1995), found that L-AP3 did not block metabotropic glutamate receptor-induced excitation of interneurones. The reason for this apparent discrepancy is not clear, but perhaps it represents a concentration effect: the frequency of spontaneous IPSCs observed by Poncer *et al.* (1995) was less than 10 Hz, rather than the > 35 Hz frequencies of gamma tails (Fig. 8).

Several important questions concerning interneurone network gamma and its relation to theta rhythm remain open. (a) Which particular interneuronal types are involved in the generation of which rhythms (Gulyás *et al.* 1993; Buhl *et al.* 1994; Sik *et al.* 1995)? (b) How exactly are the respective interneuronal subpopulations driven? (c) What is the role of subcortical structures (e.g. septal nuclei) in giving rise to widespread gamma activity?

Conclusion

Much of the interest in gamma-frequency oscillations stems from their proposed relevance to cortical information processing (reviewed by Gray, 1994). Many of the 'cognitive' issues are difficult to address experimentally involving, as they do, large aggregates of neurones *in vivo*. A thorough understanding of the cellular mechanisms of

gamma oscillations, based on recordings in brain slices and in animals, as well as on network simulations, is important for cognitive questions. An understanding of the factors involved in turning the rhythm on and off, in determining its frequency, synchrony and temporal stability, should provide tools for manipulating the rhythm *in vivo*, and thereby better assessing its functional role (Buzsáki & Chrobak, 1995).

Bragin, A., Jandó, G., Nádasdy, Z., Hetke, J., Wise, K. & Buzsáki, G. (1995). Gamma (40–100 Hz) oscillation in the hippocampus of the behaving rat. *Journal of Neuroscience* **15**, 47–60.

Buhl, E. H., Halasy, K. & Somogyi, P. (1994). Diverse sources of hippocampal unitary inhibitory postsynaptic potentials and the number of synaptic release sites. *Nature* **368**, 823–828.

Buzsáki, G. & Chrobak, J. J. (1995). Temporal structure in spatially organized neuronal ensembles: a role for interneuron networks. *Current Opinion in Neurobiology* **5**, 504–510.

Buzsáki, G., Gage, F. H., Czopf, J. & Björklund, A. (1987). Restoration of rhythmic slow activity (θ) in the subcortically denervated hippocampus by fetal CNS transplants. *Brain Research* **400**, 334–347.

Buzsáki, G., Leung, L.-W. S. & Vanderwolf, C. H. (1983). Cellular bases of hippocampal EEG in the behaving rat. *Brain Research* **287**, 139–171.

Gray, C. M. (1994). Synchronous oscillations in neuronal systems: mechanisms and functions. *Journal of Computational Neuroscience* **1**, 11–38.

Gulyás, A. I., Miles, R., Hájos, N. & Freund, T. F. (1993*a*). Precision and variability in postsynaptic target selection of inhibitory cells in the hippocampal CA3 region. *European Journal of Neuroscience* **5**, 1729–1751.

Gulyás, A. I., Miles, R., Sik, A., Tóth, K., Tamamaki, N. & Freund, T. F. (1993*b*). Hippocampal pyramidal cells excite inhibitory neurons through a single release site. *Nature* **366**, 683–687.

Leung, L. S. (1987). Hippocampal electrical activity following local tetanization. I. Afterdischarges. *Brain Research* **419**, 173–187.

McBain, C. J., DiChiara, T. J. & Kauer, J. A. (1994). Activation of metabotropic glutamate receptors differentially affects two classes of hippocampal interneurons and potentiates excitatory synaptic transmission. *Journal of Neuroscience* **14**, 4433–4445.

Macdonald, R. L. & Olsen, R. W. (1994). $GABA_A$-receptor channels. *Annual Review of Neuroscience* **17**, 569–602.

Michelson, H. B. & Wong, R. K. S. (1994). Synchronization of inhibitory neurones in the guinea pig hippocampus *in vitro*. *Journal of Physiology* **477**, 35–45.

Miles, R. (1990). Synaptic excitation of inhibitory cells by single CA3 hippocampal pyramidal cells of the guinea-pig *in vitro*. *Journal of Physiology* **428**, 61–77.

Miles, R. & Poncer, J.-C. (1993). Metabotropic glutamate receptors mediate a post-tetanic excitation of guinea-pig hippocampal inhibitory neurones. *Journal of Physiology* **463**, 461–473.

Miles, R. & Wong, R. K. S. (1987*a*). Inhibitory control of local excitatory circuits in the guinea-pig hippocampus. *Journal of Physiology* **388**, 611–629.

Miles, R. & Wong, R. K. S. (1987*b*). Latent synaptic pathways revealed after tetanic stimulation in the hippocampus. *Nature* **329**, 724–726.

Pearce, R. A. (1993). Physiological evidence for two distinct $GABA_A$ responses in rat hippocampus. *Neuron* **10**, 189–200.

Perouansky, M. & Yaari, Y. (1993). Kinetic properties of NMDA receptor-mediated synaptic currents in rat hippocampal pyramidal cells *versus* interneurones. *Journal of Physiology* **465**, 223–244.

Poncer, J.-C., Shinozaki, H. & Miles, R. (1995). Dual modulation of synaptic inhibition by distinct metabotropic glutamate receptors in the rat hippocampus. *Journal of Physiology* **485**, 121–134.

Sah, P., Hestrin, S. & Nicoll, R. A. (1990). Properties of excitatory postsynaptic currents recorded *in vitro* from rat hippocampal interneurones. *Journal of Physiology* **430**, 605–616.

Sik, A., Penttonen, M., Ylinen, A. & Buzsáki, G. (1995). Hippocampal CA1 interneurons: an *in vivo* intracellular labeling study. *Journal of Neuroscience* **15**, 6651–6665.

Sik, A., Tamamaki, N. & Freund, T. F. (1993). Complete axon arborization of a single CA3 pyramidal cell in the rat hippocampus, and its relationship with postsynaptic parvalbumin-containing interneurons. *European Journal of Neuroscience* **5**, 1719–1728.

Sloviter, R. S. (1991). Permanently altered hippocampal structure, excitability, and inhibition after experimental status epilepticus in the rat: the 'dormant basket cell' hypothesis and its possible relevance to temporal lobe epilepsy. *Hippocampus* **1**, 41–66.

Soltesz, I. & Deschênes, M. (1993). Low- and high-frequency membrane potential oscillations during theta activity in CA1 and CA3 pyramidal neurons of the rat hippocampus under ketamine-xylazine anesthesia. *Journal of Neurophysiology* **70**, 97–116.

Spruston, N., Schiller, Y., Stuart, G. & Sakmann, B. (1995). Activity-dependent action potential invasion and calcium influx into hippocampal CA1 dendrites. *Science* **268**, 297–300.

Thurbon, D., Field, A. & Redman, S. (1994). Electrotonic profiles of interneurons in stratum pyramidale of the CA1 region of rat hippocampus. *Journal of Neurophysiology* **71**, 1948–1958.

Traub, R. D. (1995). Model of synchronized population bursts in electrically coupled interneurons containing active dendritic conductances. *Journal of Computational Neuroscience* **2**, 283–289.

Traub, R. D., Colling, S. B. & Jefferys, J. G. R. (1995). Cellular mechanisms of 4-aminopyridine-induced synchronized after-discharges in the rat hippocampal slice. *Journal of Physiology* **489**, 127–140.

Traub, R. D., Jefferys, J. G. R., Miles, R., Whittington, M. A. & Tóth, K. (1994). A branching dendritic model of a rodent CA3 pyramidal neurone. *Journal of Physiology* **481**, 79–95.

Traub, R. D., Jefferys, J. G. R. & Whittington, M. A. (1994). Enhanced NMDA conductances can account for epileptiform activities induced by low Mg^{2+} in the rat hippocampal slice. *Journal of Physiology* **478**, 379–393.

Traub, R. D., Jefferys, J. G. R., Whittington, M. A., Buzsáki, G., Penttonen, M. & Colling, S. B. (1995). Models of gamma ('40 Hz') and theta rhythm in the rat hippocampus *in vitro* and *in vivo*. *Society for Neuroscience Abstracts* **21**, 1205.

Traub, R. D. & Miles, R. (1995). Pyramidal cell-to-inhibitory cell spike transduction explicable by active dendritic conductances in inhibitory cell. *Journal of Computational Neuroscience* **2**, 291–298.

Traub, R. D., Miles, R. & Jefferys, J. G. R. (1993). Synaptic and intrinsic conductances shape picrotoxin-induced synchronized after-discharges in the guinea-pig hippocampal slice. *Journal of Physiology* **461**, 525–547.

WANG, X.-J. & RINZEL, J. (1993). Spindle rhythmicity in the reticularis thalami nucleus: synchronization among mutually inhibitory neurons. *Neuroscience* **53**, 899–904.

WHITTINGTON, M. A. & JEFFERYS, J. G. R. (1995). Epileptic activity outlasts disinhibition after intrahippocampal tetanus toxin in the rat. *Journal of Physiology* **481**, 593–604.

WHITTINGTON, M. A., TRAUB, R. D. & JEFFERYS, J. G. R. (1995*a*). Synchronized oscillations in interneuron networks driven by metabotropic glutamate receptor activation. *Nature* **373**, 612–615.

WHITTINGTON, M. A., TRAUB, R. D. & JEFFERYS, J. G. R. (1995*b*). 40 Hz oscillations as a consequence of metabotropic glutamate receptor activation and $GABA_B$ergic disinhibition. *Brain Research Association Abstracts* **12**, 81.

YLINEN, A., BRAGIN, A., NÁDASDY, Z., JANDÓ, G., SZABÓ, I., SIK, A. & BUZSÁKI, G. (1995*a*). Sharp wave-associated high frequency oscillation (200 Hz) in the intact hippocampus: network and intracellular mechanisms. *Journal of Neuroscience* **15**, 30–46.

YLINEN, A., SOLTÉSZ, I., BRAGIN, A., PENTTONEN, M., SIK, A. & BUZSÁKI, G. (1995*b*). Intracellular correlates of hippocampal theta rhythm in identified pyramidal cells, granule cells and basket cells. *Hippocampus* **5**, 78–90.

Acknowledgements

This work was supported by IBM, the Human Frontier Science Program, National Institute of Neurological Diseases and Stroke (NS34994 to G.B.), the National Science Foundation, and The Wellcome Trust. J.G.R.J. was a Wellcome Trust Senior Lecturer. We thank Dr Robert Walkup for help with the IBM SP1 at the T. J. Watson Research Center, and Drs Richard Miles, Robert K. S. Wong and Ben W. Strowbridge for helpful discussions. Some simulations were performed on the IBM SP2 at the Maui High Performance Computing Center, sponsored by the Phillips Laboratory, Air Force Materiel Command, USAF, under cooperative agreement number F29601-93-2-0001. The US Government is authorized to reproduce and distribute reprints notwithstanding any copyright notation thereon. The views and conclusions contained in this document are those of the authors and should not be interpreted as necessarily representing the official policies or endorsements, either expressed or implied, of Phillips Laboratory or the US Government.

Authors' present address

J. G. R. Jefferys & S. B. Colling: Department of Physiology, The Medical School, University of Birmingham, Birmingham B15 2TT, UK.

Author's e-mail address

R. D. Traub: traub@watson.ibm.com

Received 21 September 1995; accepted 10 January 1996.